SYSTEM IDENTIFICATION OF E-VTOL ROTOR IN VORTEX RING STATE BY VISCOUS VORTEX PARTICLE METHOD

Murat Şenipek, murat.senipek@tai.com.tr, PhD. Candidate & Aeromechanics Chief Engineer,
Ilgaz Doğa Okcu, iokcu@tai.com.tr, PhD. Candidate & Flight Mechanics Chief Engineer,
Middle East Technical University & Turkish Aerospace Inc. (Turkey)
Ozan Tekinalp, tekinalp@metu.edu.tr, Professor, Middle East Technical University (Turkey)
Kemal Leblebicioğlu, kleb@metu.edu.tr, Professor, Middle East Technical University (Turkey)

Abstract

This paper presents a methodology that identifies a state-space rotor inflow model for a 1.5-m radius two bladed eVTOL rotor in descent. Main purpose of the work is to identify a state-space model for an isolated rotor for all descent envelope especially in vortex ring state condition by mid-fidelity aeromechanics analysis framework. Mid-fidelity simulation framework includes Viscous Vortex Particle Method (VVPM) accelerated by GPU coupled with a Generic Air Vehicle Model (GAVM) which is a mathematical model for analysis of generic configurations such as propeller aircrafts, conventional and unconventional rotorcrafts, multi-rotor and tiltrotor eVTOL configurations. Vortex ring state (VRS) envelopes are investigated by VVPM for full combination of several descent rates, forward velocities, collective pitch and rotational speed. VRS envelopes are visualized in terms of level of thrust and oscillatory loads to determine the critical flight conditions in terms of flight control. Instabilities, and rotor performance are discussed in detail. System identification of an isolated rotor is performed by VVPM simulations for collective frequency sweeps. Rotor performance in steep descent, system identification results, nonlinearities, unsteady aerodynamics and modeling methodologies are discussed in detail.

1. INTRODUCTION

Urban mobility operations require safe landing trajectories for all possible landing envelopes that can be defined with combinations of vertical rate of descent and translational velocity. In addition to confined landing areas, there may be local winds and gusts that push the eVTOL aircraft to their limits. Furthermore, noise requirements are also another concern while operating in residential areas. Therefore, it is desirable not to have any limit on vertical landing or approach in terms of translational velocity and rate of descent.

One of the most significant problems during landing is the condition of Vortex Ring State (VRS) that may occur in single or multiple rotors for a multi-rotor eVTOL aircraft.

The Vortex Ring State (VRS) is a risky and unpredictable phenomenon that occurs during approach and descending flight conditions where the vertical descent velocity is relatively high or steep descending flight path angles or maneuvering flight during approach. VRS is an unstable regime of operation that is caused by rotor blade-vortex interactions when the vertical descent velocity become comparable to rotor induced velocity.

As the rotor starts to descent, upward freestream velocity keeps the tip vortices just below the rotor disk that forms the vortex ring. With each revolution of the rotor blades, strength of the vortex ring increases until it breaks away from the rotor disk plane [1].Rotor interacts with the unsteady vertical wake structure that not only causes loss of thrust but also causes significant oscillatory loads and negative thrust gradients [2]. The severe coupling between the loads on the rotor and the aerodynamics of the complex wake may result in unpredictable rotorcraft behavior for flight control system and pilot. There is a history of helicopter accidents related to the inability of escaping from VRS onset and its effects [2].

In conventional helicopters, VRS onset boundary is described as the ratio of vertical speed to induced velocity vs. forward speed. As illustrated in Figure 1 there are mainly four types of working states exist for a rotor which are:

- Normal Working State
- Vortex Ring State
- Turbulent Wake State
- Windmill Brake State

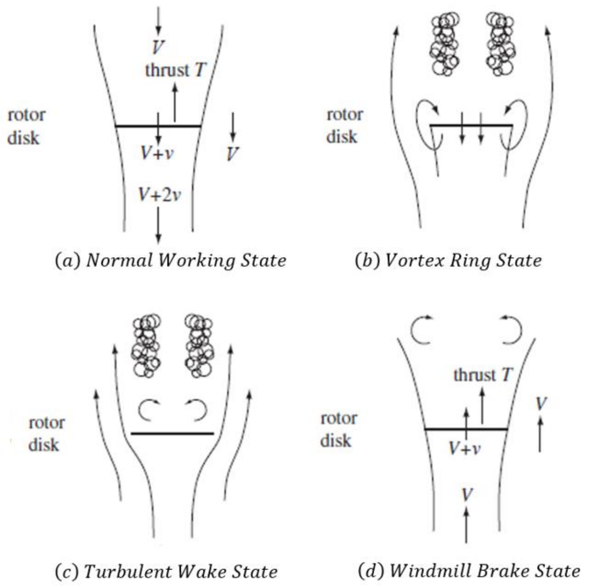

Figure 1 Working states of a rotor [1]

In normal working state, rotor operates in hover or climbing flight and wake contracts downwards and momentum theory provides good rotor performance prediction.

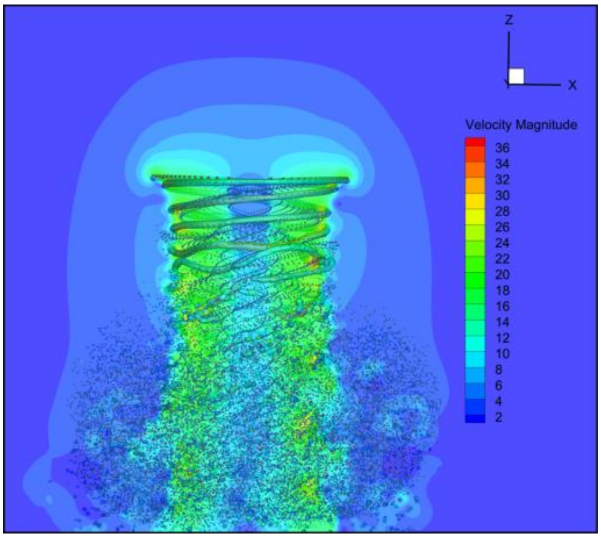

Figure 2 Rotor in Hover (VVPM Solution)

As the rotor descents beyond the rates greater than -0.5v_h, where v_h is the hover mean induced velocity, so-called vortex ring is formed in the plane of the rotor disk as illustrated in Figure 3. Since the flow on the rotor disk plane is highly unsteady and turbulent, rotor experiences high level of vibration and difficulty in controlling the descent rate due to loss of thrust.

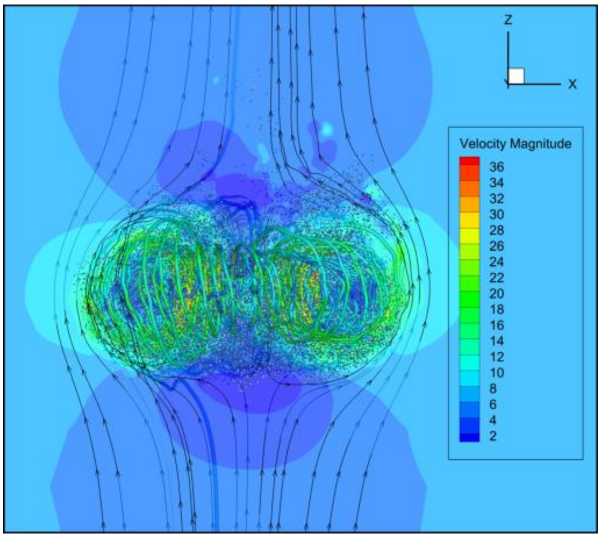

Figure 3 Rotor in VRS (VVPM Solution)

The region where vertical velocity is greater than transition velocity v_{tr} up to -2.0v_h is called as Turbulent Wake State where in general ideal autorotation occurs. In this state, the flow still has unsteadiness and turbulence, but vibration levels are reduced when compared to VRS.

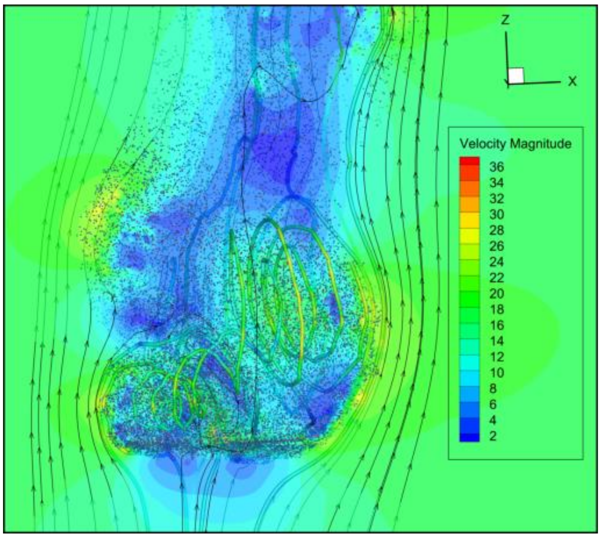

Figure 4 Rotor in Turbulent Wake State (VVPM Solution)

Windmill brake state where the descent rate is greater than -2.0v_h flow becomes smooth and velocity is upwards through the rotor disk. Momentum theory provides a good estimate and the rotor produces net power. Flowfield is illustrated in Figure 5 where smooth streamlines exist through rotor.

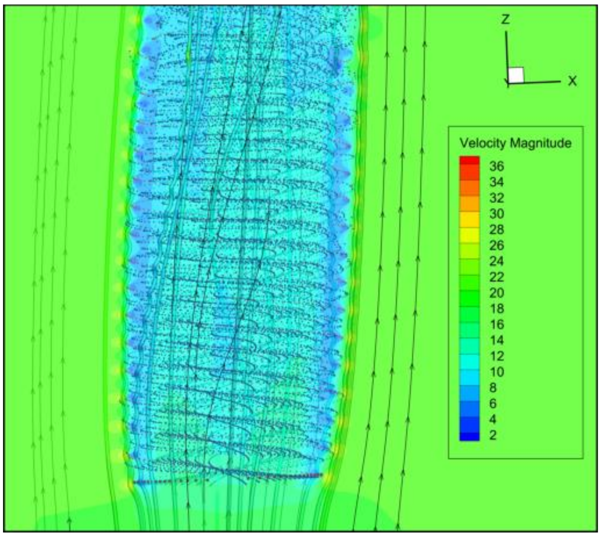

Figure 5 Rotor in Windmill Brake State (VVPM Solution)

Summary of the rotor working states in descent is as follows.

- *Normal Working State* $\frac{V_z}{V_h} \geq 0$
- *Vortex Ring State* $\frac{V_{tr}}{V_h} \leq \frac{V_z}{V_h} \leq 0$
- *Turbulent Wake State* $-2 \leq \frac{V_{tr}}{V_h} \leq 0$
- *Windmill Brake State* $\frac{V_z}{V_h} \leq 0$

For multiple rotor vehicles, hazardous situations may occur if one or more rotors operate inside this boundary that have significant thrust loss and/or negative thrust gradients. Loss of thrust suddenly causes a vertical descent for a conventional helicopter and generates a sudden moment imbalance for multi-rotor air vehicles. Having non-positive $\partial T/\partial \theta_0$ and $\partial T/\partial \Omega$ gradients not only create loss of thrust force but also creates undesired moments on the aircraft center of gravity if rotors are located at a distant location from the aircraft center of gravity. Besides, high level of vibration reduces the passenger comfort and flight quality together with an increased level of rotor noise.

Therefore, it is significant to show the adverse effects that may be observed due to VRS flight regimes for the descent conditions by simulation and/or testing.

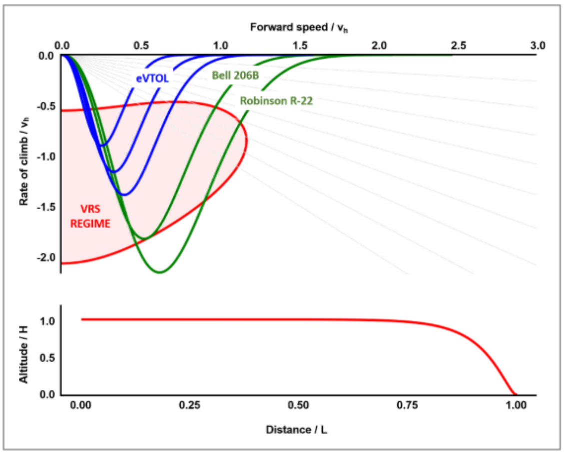

Figure 6 VRS regime for steep descent for different VTOL aircrafts. Retrieved from reference [2].

Classical VRS regime is illustrated in Figure 6 representing “steep descent” during landing. Utilizing RPM or collective pitch control may result in different VRS envelopes and characteristics. During the design phase, all possible combinations of horizontal and vertical speed should be investigated in terms of VRS encounters and it is important to minimize the adverse effects on the aircraft control system during approach due to VRS. Advanced eVTOL configurations employ several rotors and partial VRS encounters may be observed. Therefore, it is critical to determine the VRS boundaries for isolated rotors and reflect the isolated rotor characteristics into multi-rotor configurations.

Flight control system of the aircraft is desired to provide safe descent in all possible landing trajectories that require a control design considering VRS flight conditions. A means of analysis or testing environment is required to develop control systems ensuring safe approach for multi-rotor air vehicles. Wind tunnel testing may be performed to observe limits of the designed rotor in terms of VRS related problems. Furthermore, high fidelity CFD modeling may be performed but computational power will be significantly high to analyze VRS envelope and perform frequency sweep analyses for system identification. Instead of high-fidelity analyses, system identification and linearized inflow models are preferred for modern rotorcraft configurations [3].

Mid-fidelity aerodynamic analysis methods such as VVPM are inherently suitable meshless methods for rotor VRS analysis. Advancements in graphical processing unit (GPU) computing technology and various development environments, these mid-fidelity methods became much more efficient than before.

Both the VRS envelope and system identification tasks can be modeled and analyzed by VVPM based analysis.

VVPM is a Lagrangian Navier-Stokes (in vorticity transport form) solver based on first principles and it preserves coherent vortex structures for long distances and does not have any ad-hoc modeling parameters. Vorticity particles are generated from trailing edges of rotor blades and are convected into domain. Calculation of induced velocity is efficient, and it inherently includes blade-vortex interactions.

Considering VVPM as a meshless method and having GPU-compatible structure, it provides a unique opportunity to perform comprehensive analysis and even simulation to assess the wake dynamics and interference effects [4].

Although VVPM is a complex nonlinear solver, it is theoretically possible to obtain linear time invariant (LTI) models from VVPM results by system identification methods [5]. These LTI models than can be used to understand the descending propeller dynamics more comprehensively by using linear system theory tools or to come up with control algorithms that can be used to track a certain thrust level or torque level under varying conditions. Considering a descending rotor has several different working states that has different distinct characteristics, it is more convenient to come up several different linear models that uniquely capture each working phases dynamics around a selected states' trim condition.

This work utilizes thrust contour maps and frequency domain system identification to obtain linear models. The thrust contour maps are generated by trimming the VVPM model under different working conditions in terms of rate of descent and horizontal velocity with different RPM and collective settings. $\partial T/\partial \theta_0$ and $\partial T/\partial \Omega$ gradients are obtained and inspected with these analyses. Frequency domain dynamic system identification is performed for a selected number of cases to come up with the transfer functions for responses from collective to thrust and from collective to mean inflow. Frequency domain methods were preferred because of their ease of use, their ability to give insight about the underlying dynamics by frequency response functions without the need of a parametrized LTI model structure, computational efficiency and their rich literature about rotary wing system identification applications [5]–[7].

The LTI models need to be able to capture primarily the dynamics of the air mass; thus, inflow states should appear explicitly in the model states. To this end, inflow states are calculated and taken as output from the VVPM solutions. Apart from the inflow states thrust levels was the other concern; thus, each system identification run set up such that thrust and uniform mean inflow are saved so their dynamic behavior could be inspected. The system identification simulations utilize the frequency sweep input and each analyzed case was simulated twice to cover the low frequency region of interest and higher frequency regions. For validation, step input runs from collective input to mean inflow state were performed.

In this work, GPU accelerated VVPM code is utilized to determine the VRS boundaries for collective pitch and RPM inputs for a 1.5-m radius eVTOL rotor. In addition, collective frequency sweep analyses are performed to identify the LTI models. The purpose of this work is to investigate the VRS regime for a single rotor and perform system identification of low-speed descent condition for a collective pitch actuated rotor.

2. METHODOLOGY

In this part, the methodology of the work is presented. VVPM analysis framework is utilized to investigate the VRS boundaries for both collective pitch actuated rotor and for rotational speed actuated rotor. Analysis conditions are determined for different descent flight path angles, collective pitch, and RPM inputs. Rotor thrust, oscillatory loads, inflow approximations are monitored. The main purpose is to illustrate the VRS behavior of rotors with different actuation mechanisms. Then, critical conditions are selected from the VRS envelope for system identification tasks. Finally, system identification tasks are performed, and significant issues are discussed.

2.1. VVPM Coupled Generic Air Vehicle Model

The Generic Air Vehicle Model (GAVM) is developed to perform quick analysis and simulations of a generic rotorcraft configurations [8]. Conventional propeller airplanes, conventional and modern helicopters such as compound and tiltrotors can be modeled and simulated.

VVPM is a Lagrangian Navier-Stokes (in vorticity transport form) solver based on first principles and it preserves coherent vortex structures for long distances and does not have any ad-hoc modeling parameters. Vorticity particles are generated from trailing edges of rotor blades and are convected into domain. Calculation of induced velocity is efficient and it inherently includes rotor-rotor interactions. All of these inherent advantages make the vortex particle method a natural candidate to solve the vorticity dominated incompressible flow-field around rotorcraft configurations [9] In this work, inviscid vortex particle method is used in validation and simulation cases that only solves explicit convection part of the governing equation.

$$\frac{d\vec{x}_i}{dt} = \vec{u}_i = -\sum_{j=1}^{N} \frac{1}{\sigma_{ij}^3} K(\rho)(\vec{x}_i - \vec{x}_j) \times \vec{\alpha}_j \tag{1}$$

Solving above equation requires the induced contributions from all the particles to calculate the induced velocity of a particle $\vec{u}_i$ that makes the VPM traditional N-body problem [10]. Therefore, it is very feasible to implement it in a GPU environment for parallelization. Implementation of GPU algorithm in CUDA reduces the solution time from 9 hours to 5 minutes for a desktop computer. Several validation cases are published varying from isolated rotor to full helicopter cases. [4]

An experimental case for an isolated rotor is modeled by vortex particle method to investigate the effect of rapid blade-pitch increase on the thrust and induced velocity response [11]. Rate of blade pitch increase of about 200° is applied on a 3-bladed rotor system and inflow response is compared with the experiment for 1 second.

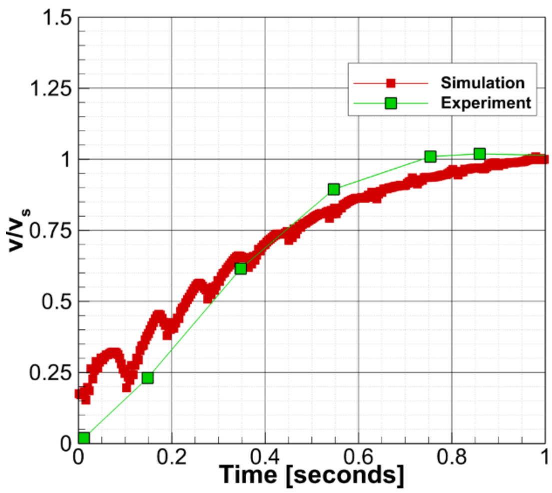

Figure 7 Time history of induced velocity after rapid pitch increase

Result is illustrated in Figure 7 where time history of the ratio of induced velocity to the value of steady state induced velocity is consistent with experiment.

Sample 1.5-m radius 2-bladed rotor rotating at nominal 1000 RPM is modeled to analyze VRS boundaries and perform system identification tasks as given in Table 1. Target rotor thrust varies between 1000 N to 2000 N in terms of sizing of the rotor.

Table 1 - Modeled Rotor Specifications

Main Rotor Parameters	
Radius [m]	1.5
Nominal Chord [cm]	25
Solidity	0.106
\# of blades	2
Nominal RPM	1000
Tip Speed [m/s]	157

2.2. Investigation of VRS Boundaries

Working states of the modeled rotor are investigated by VVPM analyses to observe the behavior of rotor for possible descent scenarios.

The first approach was to trim the rotor for a desired thrust level along the full horizontal speed and descent rate envelope. Trim can be achieved in normal working state and shallow descent conditions since the control gradients are obtained from finite state models. However, in steep descent conditions, the control gradients ($\partial T/\partial \theta_0$ and $\partial T/\partial \Omega$) from finite state models does not provide adequate convergence. Therefore, trim conditions cannot be achieved in VRS conditions.

Then, it is decided to perform wide range of envelope without trimming for a given thrust level. Wider analysis matrix is prepared to perform VRS investigation of an isolated rotor including the full combination of horizontal velocity, rate of descent, collective pitch and rotational speed. Feasible range of thrust is analyzed to predict the control ranges in terms of collective pitch and rotational speed. Following points are analyzed to observe the changes in rotor thrust, power, peak-to-peak loads and mainly the control gradients.

- $V_{level} = [0\ to\ 30]\ knots\ by\ 10\ knots\ resolution$
- $\Omega \quad = [800\ to\ 1000]\ RPM\ by\ 50\ RPM\ resolution$
- $\theta_0 \quad = [8.5\ to\ 11.5]\ degrees\ by\ 30'\ of\ resolution$
- $RoC \quad = [0\ to -5000]\ fpm\ by\ 250\ fpm\ resolution$

Total analysis matrix is four dimensional and includes 2940 points that corresponds approximately 490h of computation in NVDIA GeForce RTX2070s having 2560 CUDA cores. Single analysis has 16 revolutions with 5 degrees of azimuth corresponding to the timestep of 8.38x10-4 seconds and having ~40000 vortex particles at steady state.

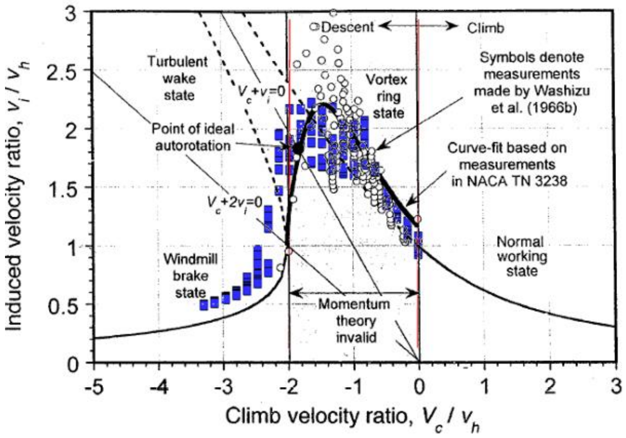

Figure 8 Induced velocity change in VRS and comparison with available data [12]

In Figure 8, ratio of induced velocity to hover induced velocity is compared with the available literature data and momentum theory for different rates of descent condition. Blue squares represent the VPM analysis results for different collective settings for a constant 900 RPM value. As seen from the figure, VRS region induced velocity ratios are consistent with the literature and provide a good estimate for rotor induced velocity. Therefore, these settings are used in VRS envelope investigation analysis campaign having 2940 analysis points.

4-Dimensional VRS envelope is used to determine the critical regions in terms of control gradient and oscillatory loads. Flight conditions of rotor system identification tasks are determined from the generated wide envelope.

2.3. Rotor System Identifikation

A good model structure that is widely used both in academia and industry is the Pitt-Peters dynamic inflow model for the entire flight envelope of a rotor shown in Eq. (2). However, for this work selected system identification points are axial climb conditions where the airflow passing through the rotor disc is mostly dominated and can be represented with the scalar counterpart of Pitt-Peters model. That is why the system identification is performed in a single-input-single-output framework.

(2) $$M\dot{\lambda} = L^{-1}\lambda = C(t-\tau)$$

SISO frequency domain system identification used in this work is adapted from reference [5] and utilizes CIFER®. As mentioned before, no parametrized model structures are required for system identification. However, after the frequency responses are obtained, a parametrization can be performed once an LTI structure is selected. The availability of the frequency response curves beforehand, allows an experienced engineer to come up with the LTI structure while gaining insight about the system dynamic behavior.

Frequency domain identification can be summarized as transforming the input-output set of a given experiment from time domain to frequency domain and with the help of spectral functions determining the frequency response of the input output pair.

The definitions for the fourier transform, the autospectral function G_{uu},the cross spectral function G_{uy} and the frequency response $G(f)$ are given in equations (3) through (5).

(3) $$U(f) = \int_{-\infty}^{\infty} u(t)e^{-j2\pi ft}dt, \quad u(t) \in \mathbb{R}^{1\times 1}$$

(4) $$G_{uu}(f) = \frac{2}{T}|U(f)|$$
$$G_{uy}(f) = \frac{2}{T}|U^*(f)Y(f)|$$

(5) $$G(f) = \frac{G_{uy}}{G_{uu}} = \frac{G_{yy}}{G_{yu}}$$

Considering Eq. (2), the relationship between collective, thrust and inflow can be put into a block diagram form like the one given in Figure 9. The simulation results obtained from VVPM solutions revealed that no dynamic phenomena occur from collective input to thrust output. High frequency excitation runs up to 400 rad/s were performed to exploit any dynamics between collective and thrust without any success. The static relationship may be explained with the lack of flapping dynamics for the propeller at hand or the unsteady aerodynamic modeling.

It s obvious from Figure 9 that if C_T and θ_0 are statically related or $\dot{C}_T = \dot{\theta}_0$, one can use the collective input excitation to reveal the dynamics between the thrust and inflow.

The system identification trim conditions were selecteed as the axial flight conditions to ease the analysis process. The VVPM model is trimmed with the previously determiend rate of climb values for the hover (Case ID 1), VRS (Case ID 2) and the windmill brake state (Case ID 3) with zero forward flight velocity. For validation step response simulations were also conducted at the same conditions.

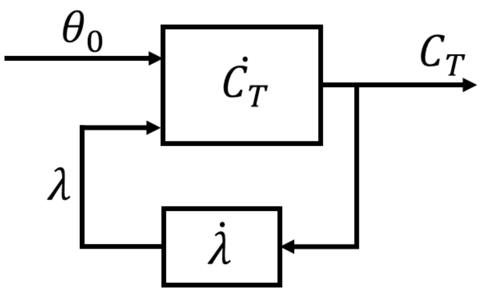

Figure 9 Collective, Thrust and Inflow Block Diagram

Table 2 Analysis cases for system identification tasks

Analysis Cases				
ID	V_{level} (knots)	RoC (ft/min)	θ_0 (degrees)	Ω (rev/min)
1	0	0	10	900
2	0	-1250	10	850
3	0	-4000	10	900

System identification inputs were designed to reveal the underlying dynamics by following the guidelines specified in Ref. [5]. Initial frequency sweeps were performed to excite 0.3-105 rad/s frequency interval. The simulation time for each run was 90 seconds. The lower end is selected as 0.3 rad/s to see if any dynamics are present in the manned rotorcraft rigid body dynamics range. Another reason to include such low frequency excitations was to make sure there is enough time for the rotor wake formations to reach a quasi-steady level. Initially, the higher end was selected to cover 1/rev frequency. Secon higher frequency runs for each case were performed to make sure the collective thrust relationships' nature and were performed from 50 rad/s to 400 rad/s as 30 second runs. The amplitude of the collective excitations is determined as 1 degrees. Two different runs for each case were merged in the CIFER® environment automatically which is performed by appending two simulation runs back-to-back in time domain before performing the fast Fourier transform.

Step responses were generated for each selected case by first time marching the simulation to the prescribed trim condition, and then introducing the step inputs.

Frequency responses for each ID case were inspected to gain an understanding about the underlying physical phenomena as stated before and for the suitable frequency responses SISO LTI model fits were obtained. The LTI models were also validated with step response analyses to further increase the confidence level to the system identification process.

3. RESULTS

VRS envelope analysis is summarized in this chapter. Sample visualizations belonging to different vertical descent conditions are provided. Vortex particles and vorticity isosurfaces are illustrated for hovering case with 10° collective pitch and 900 RPM in Figure 10. Onset of VRS condition for vertical descent is determined as -1250 fpm vertical speed and illustrated in Figure 11. It is clearly seen that the vortex ring generated by rotor is directly interacting with the rotor itself which creates an unstable condition and loss of thrust. In Figure 12, turbulent wake state is illustrated with the same collective pitch and rotational speed. Although the vortex ring is convected with upstream, unsteadiness and rotor-wake interaction generates significant oscillatory loads. In addition, it is the condition where autorotation starts.

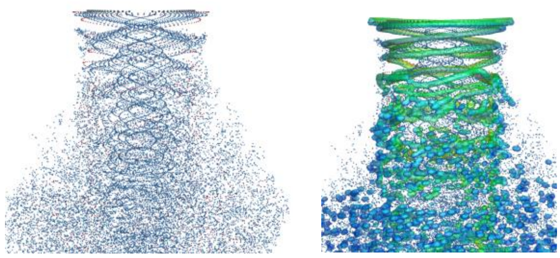

Figure 10 Normal Working State (Hover)

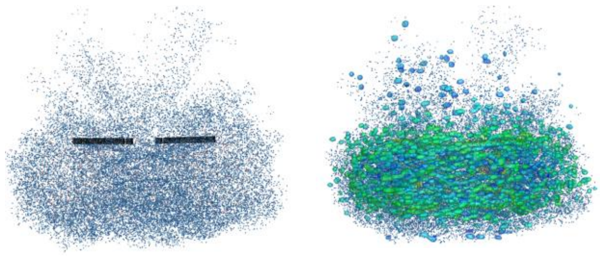

Figure 11 Onset of Vortex Ring State (Vertical descent wirth -1250 ft/min)

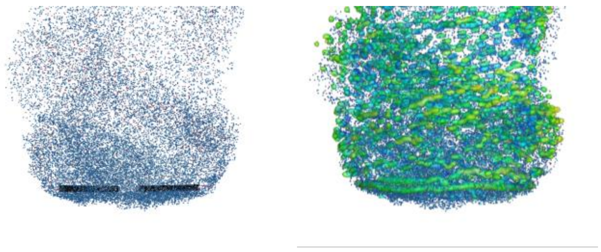

Figure 12 Turbulent wake state (Vertical descent with -3250 fpm)

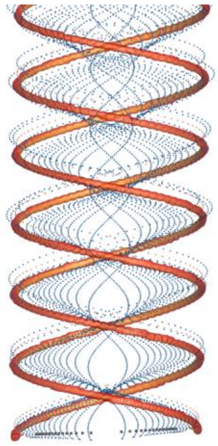

Figure 13 Windmill brake state (Vertical Descent with -8000 fpm)

In Figure 13, strong tip vortices and shed vortices move away from the rotor and leaving a clean upwash for windmill brake state. In that condition, thrust gradients are negative since most of the blade sections operate in post-stall angles of attack.

Since the sign change of $\partial T/\partial\theta_0$ or $\partial T/\partial\Omega$ is one of the main indicators of VRS encounter, analysis maps are generated to determine the locations that have severe blade vortex interactions. In Figure 14, both of $\partial T/\partial\theta_0$ and $\partial T/\partial\Omega$ have positive sign and there is no control reversal. Thrust distribution is almost linear and there is not any significant effect due to VRS.

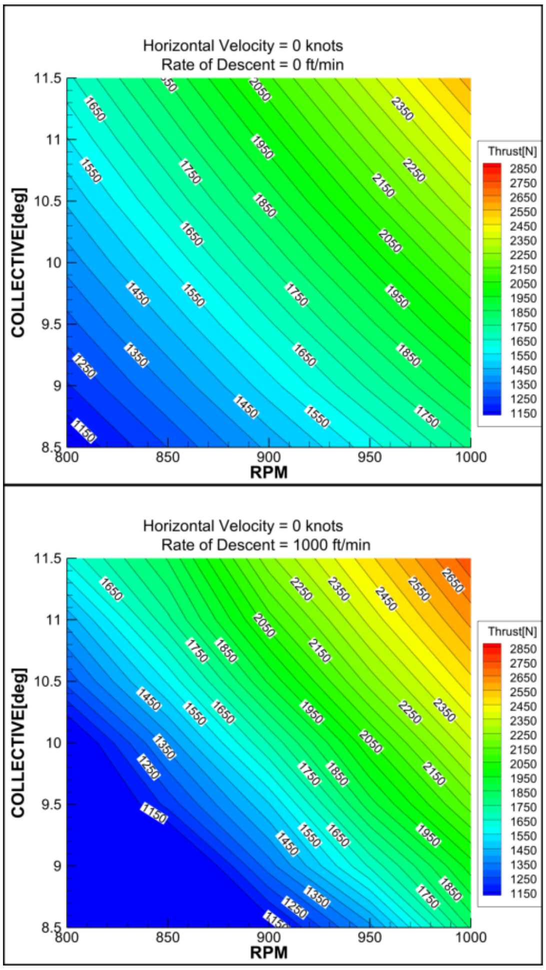

Figure 14 Thrust contour map for vertical descent as a function of θ_0 and Ω (Up: 0 fpm, Down: -1000 fpm)

In Figure 15, as the descent velocity is increased, nonlinearities are observed in thrust contours especially for 1250 fpm descent rate. Approximately 30% of thrust is lost which leads to a sudden altitude loss if the rotorcraft were descending vertically at that rate. Furthermore, any type of vertical gust may cause loss of thrust during descending near to this boundary. Besides the loss of thrust, control gradients are almost nonexistent for 1250 fpm descent case. In 4000 fpm descent case another critical condition is observed. $\partial T/\partial\theta_0$ gradients are not positive, thrust is decreased with increasing collective for certain RPM values. However, RPM control still provides positive $\partial T/\partial\Omega$ gradients.

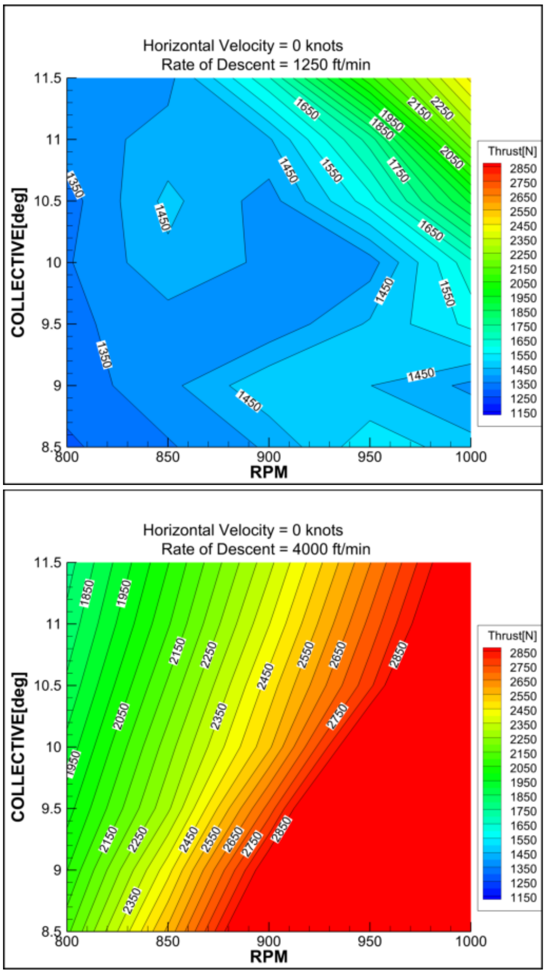

Figure 15 Thrust contour map for vertical descent as a function of θ_0 and Ω (Up: -1250 fpm, Down: -4000 fpm)

The main reason behind the difference in thrust gradients for windmill brake state is that the rotor blade sections operate in post-stall regions where increasing angle of attack no longer generates positive thrust for collective pitch controlled case. Although blade sections are operating in post-stall region increasing rotational speed increases local dynamic pressure which results in increased level of total thrust.

The apparent VRS condition in Figure 15 (up) is disappeared when the horizontal velocity is higher. Figure 16 illustrates the recovery from the VRS in terms of thrust gradients and thrust levels. This result shows that a slight forward velocity makes the rotor recover from the VRS condition if it is achieved in time.

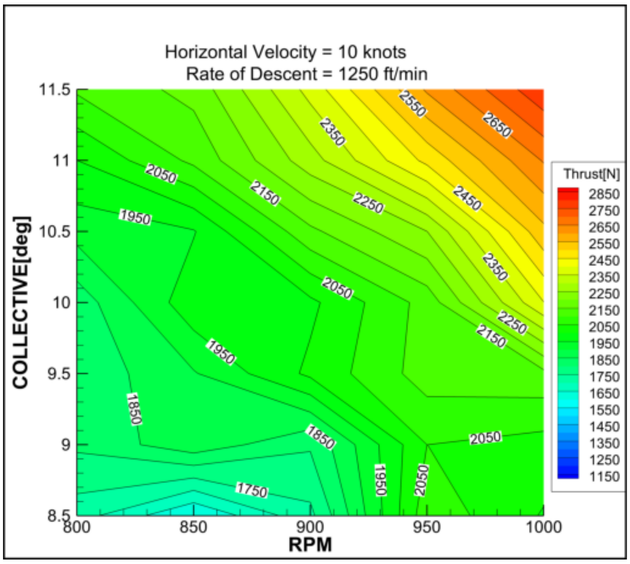

Figure 16 Thrust contour map for 1250 fpm descent at 10 knots horizontal velocity as a function of θ_0 and Ω

Constant RPM and constant collective pitch envelopes are also investigated with different rate of descent values and different forward velocities. These envelopes are provided in appendix section in Figure 30 and Figure 31. Previous results about loss of thrust region (vertical descent with approximately -1250 fpm) are observed for both envelopes. Furthermore, sign of control gradients up to 40 knots and -5000 fpm are observed. Similar results are obtained for $\partial T/\partial \theta_0$ and $\partial T/\partial \Omega$. Almost no negative thrust gradient of RPM ($\partial T/\partial \Omega$) is observed in fixed collective maps. However, negative thrust gradients exist ($\partial T/\partial \theta_0$) for steep rate of descent values in RPM fixed maps.

Summary envelopes for thrust and oscillatory loads are plotted for constant collective pitch and RPM which are 10° and 900 respectively. Critical conditions are illustrated in Figure 17 which are VRS onset where the loss of thrust occurs and windmill brake state where $\partial T/\partial \theta_0$ derivative becomes negative. In addition, peak-to-peak torque values are plotted in Figure 18 to observe any blade vortex interaction (BVI) related phenomenon and critical descent cases in terms of oscillatory loads. There is a sudden increase in oscillatory torque while entering VRS region. In windmill brake state oscillatory loads are small since there is no rotor-wake interaction and flow angle is nearly axial. Approach BVI condition is depicted in the figure where there is a sharp increase of oscillatory loads which corresponds to a situation during approach with low forward speed.

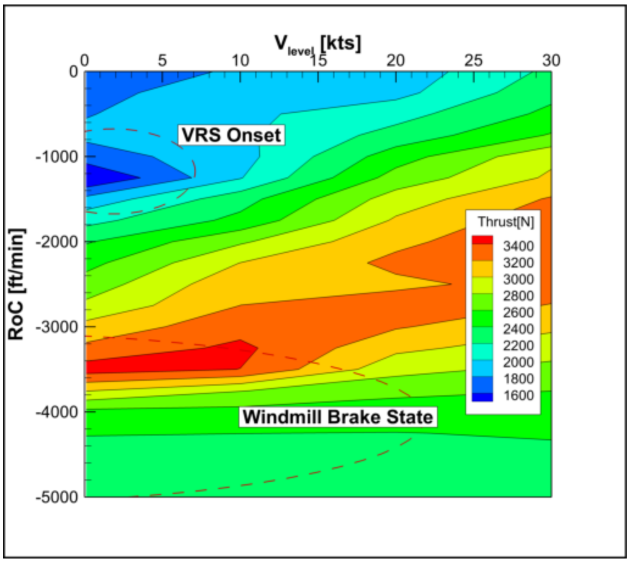

Figure 17 Thrust contours for descent and forward velocity envelope (of θ_0 and Ω $are\ fixed$)

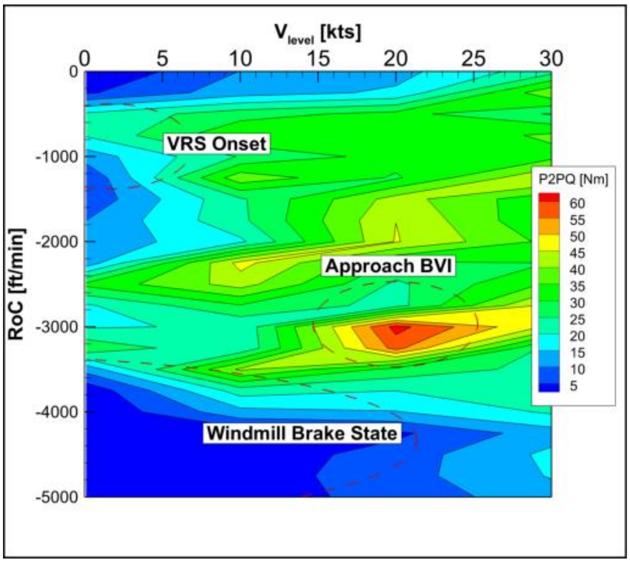

Figure 18 Peak-to-peak torque contours for descent and forward velocity envelope (of θ_0 and Ω $are\ fixed$)

Step inputs are applied to three cases which are hover (Case ID 1), VRS descent (Case ID 2) and windmill brake state (Case ID 3). Hover step input and thrust response of thrust is illustrated in Figure 19. The step input results also show the time marching part of the simulation before the VVPM model settles into a steady state trim. The step collective changes were only introduced after a steady condition is achieved to be able to inspect the linear response behavior of the VVPM model. As expected from the previous analyses and VRS envelopes, thrust gradient $\partial T/\partial\theta_0$ is positive and provides a good initial and steady state response when collective pitch step input is applied.

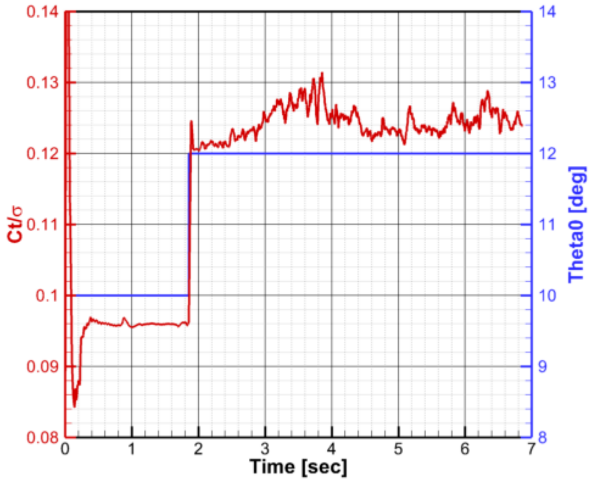

Figure 19 Thrust loading vs. time for 1° step input in θ_0 at Hover condition

It is observed that during VRS condition at 1250 fpm vertical descent, VPM solution convergence takes much more time than other conditions. That is because there is an alive vortex ring which gains strength as the rotor stays in the same condition. Therefore, a long analysis is performed for that condition and thrust coefficient vs. simulation time is illustrated in Figure 20. Thrust achieves steady state approximately after 12 seconds which corresponds to approximately 200 revolutions. Oscillatory behavior is apparent which shows the significant blade vortex interaction.

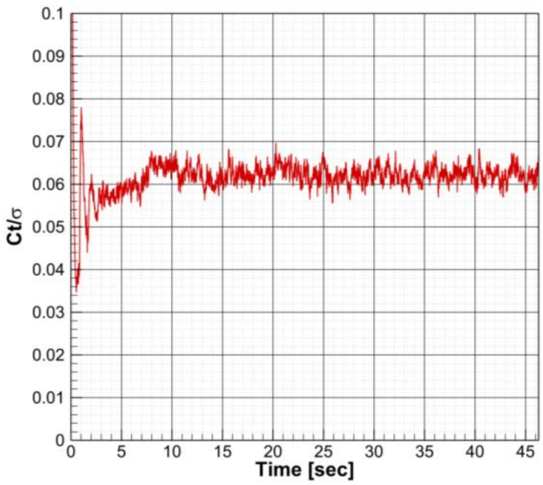

Figure 20 Thrust loading vs. time in VRS condition (-1250 fpm in vertical descent)

At t=18 seconds 1° of collective pitch step input is applied to the rotor as given in Figure 21. Although there is a rotor response initially, steady state values converge to a value that is close to the steady state trim condition thrust level. This behavior is observed in VRS envelope plots as given previously in Figure 15 (up) where there was not much sensitivity to a collective change. This is a critical issue in terms of system identification and system linearization. There is a clear nonlinearity and insensitivity of collective pitch input.

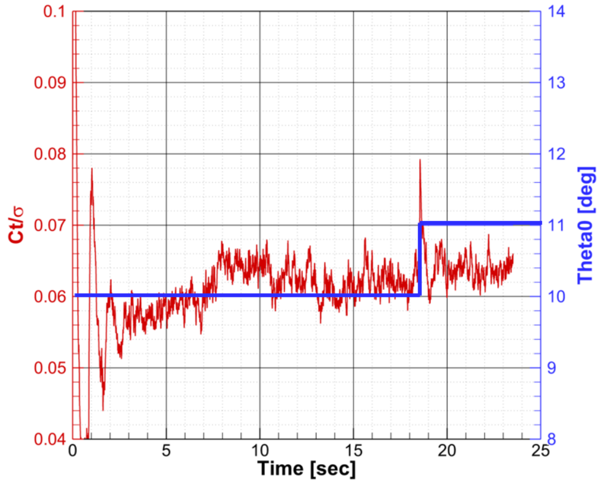

Figure 21 Thrust loading vs. time for 1° step input in θ_0 at VRS condition (-1250 fpm in vertical descent)

VRS envelopes shows that the gradient $\partial T/\partial\theta_0$ is negative in windmill brake state. Step input is applied to collective pitch to observe the rotor thrust response as given in Figure 22. Negative thrust gradient is clearly seen from the results of step input. Thrust loading decreases about 10% for a 1° of positive collective pitch step input. Another critical point is that there is almost no oscillation in thrust levels since the rotor wake moves away from the rotor plane quickly.

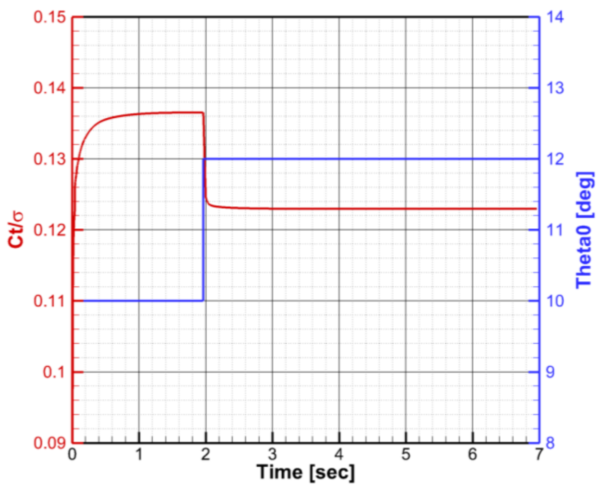

Figure 22 Thrust loading vs. time for 1° step input in θ_0 at windmill brake state (-4000 fpm in vertical descent)

System identification is initiated with frequency sweep input for cases in conditions depicted in Table 2 with the excitation signals shown in Figure 23 and Figure 24. The frequency of the sweep signals do not increase linearly with time. For better identification data at lower frequencies the frequency increase is exponentially increasing as given in equation (6). A fade-in-fade-out (FIFO) for the starting and ending portions of excitation signal is utilized. Figure 23 shows the 0.3 rad/s – 105 rad/s sweep signal input and Figure 24 shows the 50 rad/s – 400 rad/s input.

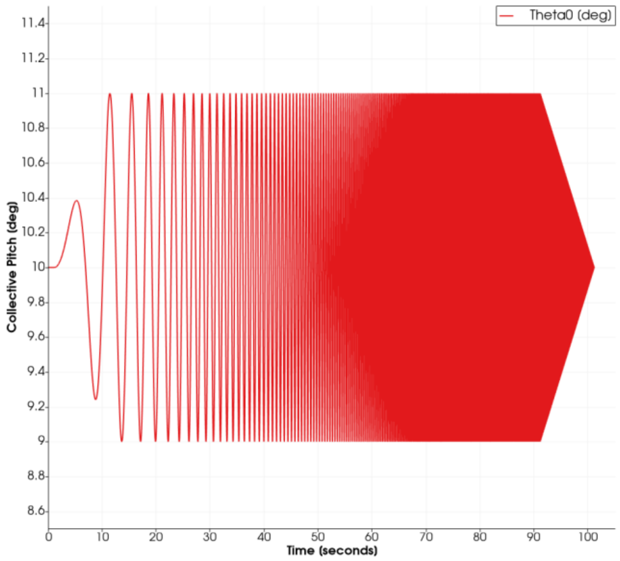

Figure 23 Low Frequency Excitation Signal for Collective Input

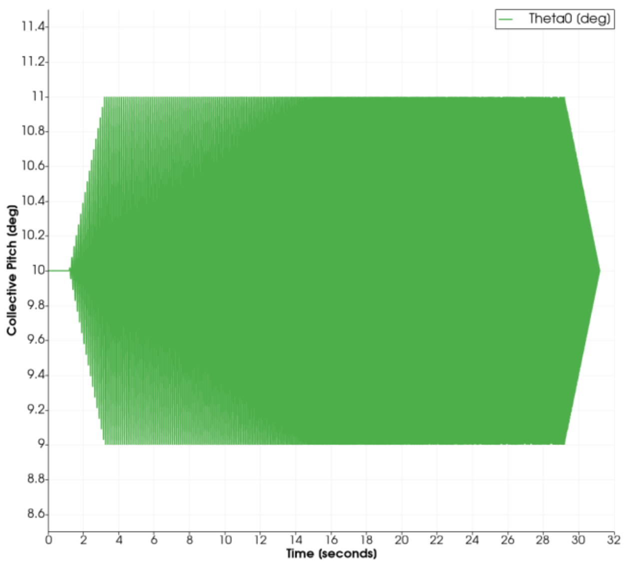

Figure 24 High Frequency Excitation Signal for Collective Input

$$\theta_0 = A \sin\left[\int_0^T \omega_{min} + K(\omega_{max} - \omega_{min})dt\right] \quad (6)$$

$$K = 0.018(e^{\frac{4t}{T}} - 1)$$

The frequency response and the transfer function fit from collective to inflow at hover for Case ID 1 is shown in Figure 25 the frequency response covers the entire frequency range whereas the transfer function fit utilizes the range up to a first order transfer function fit will be sensible. At around 0.7/rev VVPM simulations shows a notch like behavior and after that at 2/rev and 4/rev inflow response shows resonant peaks.

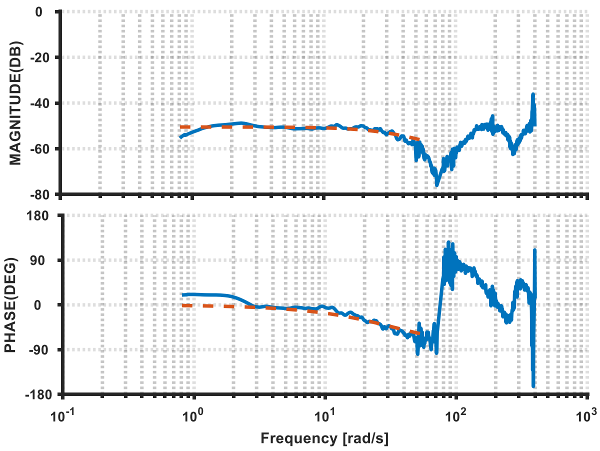

Figure 25 Frequency Response from collective to inflow and Transfer Function Fit for Hover

The step response of the mean inflow to a collective step input versus the identified LTI model response is shown in Figure 26. The initial transient response seems somewhat adequate, but the steady response seems far off. Lower frequency regions of the frequency response fit indicates that the steady behavior of inflow should have been represented well in the step response analyses as well. This indicates nonlinear dynamics are dominant in the inflow dynamics in VVPM simulations.

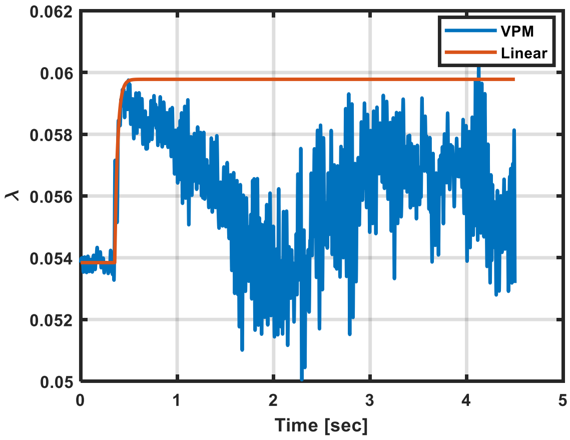

Figure 26 Inflow step response to collective at hover

VRS Frequency response is shown in Figure 27. Complementing the magnitude and phase curves Figure 27 also shows the coherence value for the input output pair in question. Lower coherence values than 0.6 are considered as an indication of poor linear relation between the input and output, collective and inflow in this case, as a rule of thumb. Although in lower frequencies there is sufficient coherence exists these results are not suitable for a transfer function estimation since, there may be dynamic content in the higher frequency region as the hover results indicate.

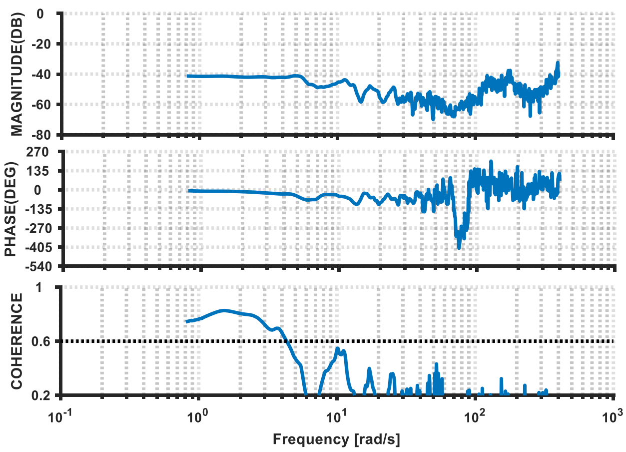

Figure 27 Frequency Response from collective to inflow and Transfer Function Fit for VRS

Figure 28 illustrates the windmill brake condition frequency response and transfer function fit. The windmill brake state results in the smoothest frequency response curves since the flow does not show any nonlinearities around this state as explained in the introduction section. The notch like behavior seen in the hover case seems to be present in the windmill brake state as well. Although the frequency and damping of the zero dipole seems to be very different from the hover case. The phase angle shows the inverse collective inflow gradient which in turn presents itself in trust step responses as well.

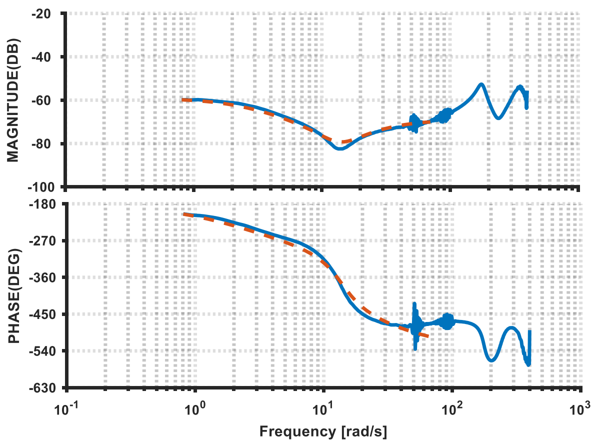

Figure 28 Frequency Response from collective to inflow and Transfer Function Fit for Windmill Brake State

The transfer function fit covers up to 70 rad/s for windmill brake case since a higher order transfer function seems unavoidable for this case. The 2/rev and 4/rev roots again present themselves in the frequency response but out of the scope for the LTI model again. The transfer function from collective to inflow has a zero dipole and a second order pole.

Step response of inflow is shown in Figure 29. The relatively low frequency behavior at the transition seems to be captured well by the linear model, however the lack of higher order poles shows themselves in the initial over shoot and the steady response as well.

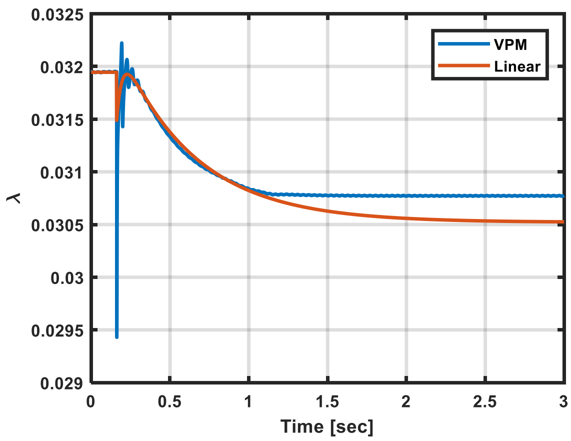

Figure 29 Inflow step response to collective at Windmill Brake State

For a better step response fit it is necessary to increase the transfer function order.

4. REMARKS

In this paper, extensive simulations are performed by using a mid-fidelity vortex particle-based aerodynamics rotor solver. GPU compatibility provides a huge advantage in terms of computational cost of the analyses. Working states of rotor in descent conditions are investigated in detail. Validation with available experimental data is performed for VRS and rapid pitch change of a rotor in hover. It is concluded that VPM based analysis provides adequate accuracy in terms of predicting the Vortex Ring State.

More than 3000 flight conditions are analyzed with VVPM to depict the VRS envelope in terms of descent rate, forward speed, collective pitch and RPM. Significant non-linearities are observed in VRS conditions. The most significant sign of the VRS is observed as the loss of thrust to almost 30%. Furthermore, increased levels of oscillatory loads are observed during approach descent conditions where there is BVI phenomena. Another clear observation is made on the negative sign of the gradient $\partial T/\partial \theta_0$ during windmill brake state.

Observations based on VRS envelopes are checked with applying step inputs in hover, VRS and Windmill Brake state conditions. In hover, there is a positive control derivative as expected. In VRS, the response was not linear and its effect quickly dies out which means that there is not enough control authority in terms of collective pitch. In windmill brake state, step input response validates the VRS envelope results since the control derivatives are negative due to stalled region of rotor blade sections.

In this work, system identification is performed only using collective pitch. Future work is planned on RPM and multi-input multi-output system identification.

During the system identification frequency sweeps, it is observed that there is no dynamic between collective pitch and thrust at high frequency oscillations. That is an expected result since the airloads model in VPM is based on quasi steady aerodynamics that utilizes 2-D (α, M) viscous static airfoil tables. Unsteady aerodynamics are classified into three main group in terms of motion frequency which are [13];

- Quasi-Steady Aerodynamics (1Hz or below)

- Quasi-Unsteady Aerodynamics (5-15 Hz)
- Unsteady Aerodynamics (~40 Hz)

Existing dynamics are the inflow and wake dynamics which are at low frequencies. For the future work, airloads dynamics will be implemented into airloads model as attached flow unsteady aerodynamics and dynamic stall models. Furthermore, vortex particle generation should be modeled consistent with unsteady air loads modeling.

Inflow dynamics present themselves as a first order model hover and a second order model with Windmill brake conditions. Both hover and windmill brake cases show there is significant dynamic content related with 2/rev and 4/rev frequencies as well. These higher dynamics require higher state models to be captured. It is also important to note that for both hover and windmill brake case a zero dipole appears and dominates the transient response for a step input.

It was not possible to fit a LTI model structure to VRS frequency response since the coherence levels were low. A special kind of sys id input with a higher magnitude and a carefully selected frequency range of interest should be used to come up with a meaningful frequency response for the VRS case.

Further investigation requires higher amplitude excitation signals to avoid low coherence, higher order LTI models to be able to capture higher order flow dynamics better and analysis of the forward flight conditions with the inclusion of inflow states other than the mean inflow.

5. REFERENCES

[1] W. Johnson, *Rotorcraft Aeromechanics*, vol. 9781107028. 2006.

[2] R. E. Brown, “Are eVTOL Aircraft inherently more susceptible to the Vortex Ring State than Conventional Helicopters ?,” in *48th European Rotorcraft Forum*, 2022.

[3] et. al. Jeffrey D. Keller, “Linearized Inflow and Interference Models from High Fidelity Free Wake Analysis for Modern Rotorcraft Configurations,” in *Vertical flight Society 76th Forum*, 2020.

[4] M. Şenipek, O. Güngör, and O. Tekinalp, “Development and Validation of a Fast Mid-Fidelity Comprehensive Analysis Tool for Generic E-Vtol Configurations,” in *48th European Rotorcraft Forum*, 2022.

[5] M. B. Tischler and R. K. Remple, *Aircraft and Rotorcraft System Identification Engineering Methods with Flight-Test Examples*. 2012.

[6] V. Klein and E. A. Morelli, *Aircraft System Identification Theory and Practice*. American Institute of Aeronautics and Astronautics, Inc., 2006.

[7] R. V. Jategaonkar, *Flight Vehicle System Identification : A Time Domain Methodology*. American Institute of Aeronautics and Astronautics, Inc., 2006.

[8] M. Şenipek, “Development of an Object-Oriented Design, Analysis and Simulation Software for a Generic Air Vehicle,” METU, 2017.

[9] J. Zhao and C. He, “A viscous vortex particle model for rotor wake and interference analysis,” *J. Am. Helicopter Soc.*, vol. 55, no. 1, 2010.

[10] J. Zhao and C. He, “A hybrid solver with combined CFD and viscous vortex particle method,” in *Annual Forum Proceedings - AHS International*, 2011, vol. 1.

[11] P. Carpenter and B. Fridovich, “Effect of a Rapid Blade-Pitch Increase on the Thrust and Induced-Velocity Response of a Full-Scale Helicopter Rotor,” *NASA Tech. Memo.*, vol. 16, no. 6, 1953.

[12] G. J. Leishmann, “Principles of Helicopter Aerodynamics.” .

[13] Ü. Gülçat, *Fundamentals of Modern Unsteady Aerodynamics*. 2021.

6. APPENDIX

Thrust contours are plotted for different forward velocities at constant RPM at 900 rev/min.

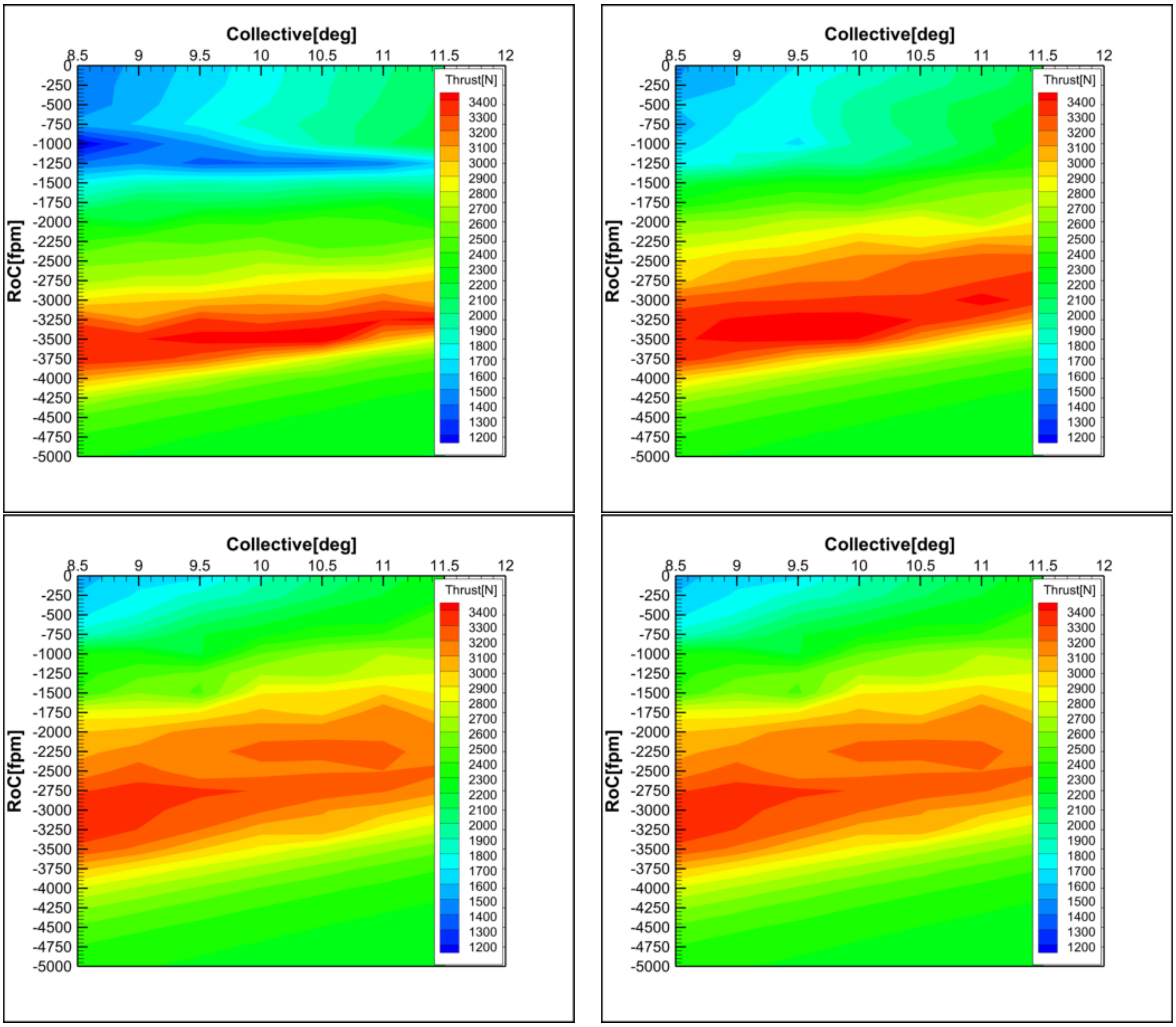

Figure 30 Thrust contours for a collective pitch vs. descent rate range for different forward velocities

Thrust contours are plotted for different forward velocities at constant collective pitch at 10°.

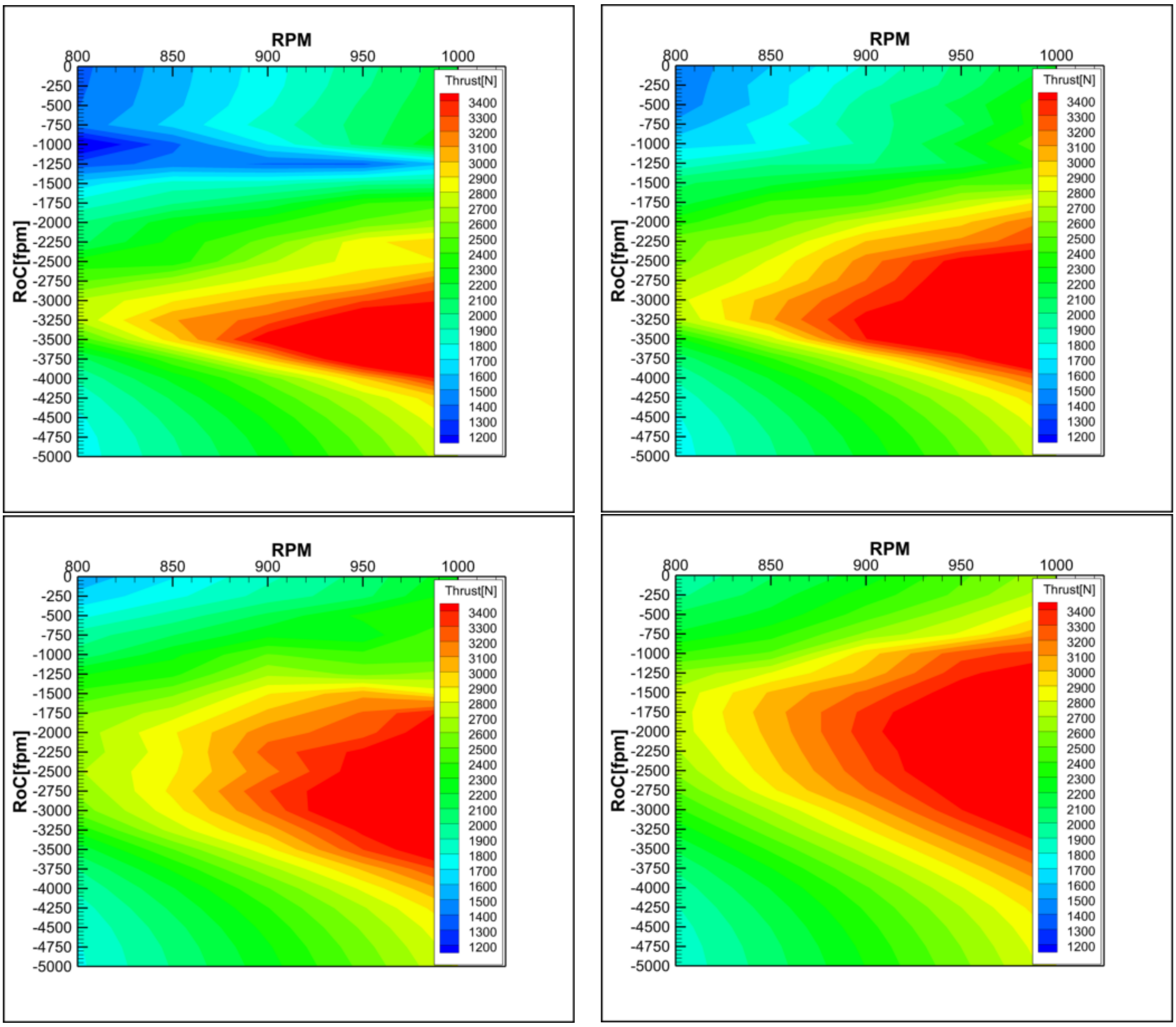

Figure 31 Thrust contours for RPM vs. descent rate range for different forward velocities